The role of hydrogen plasma power on surface roughness and carrier transport in transfer-doped H-diamond

Kevin G. Crawford,[1,a)] Alexandre Tallaire,[2] Xu Li,[1] David A. Macdonald,[1] Dongchen Qi,[3] and David A. J. Moran[1]

1 School of Engineering, University of Glasgow, Glasgow G12 8LT, United Kingdom
2 LSPM-CNRS, Université Paris 13, Villetaneuse 93430, France
3 Department of Chemistry and Physics, La Trobe Institute for Molecular Science, La Trobe University, Melbourne, Victoria 3086, Australia
a) Electronic Mail: k.crawford.2@research.gla.ac.uk

Surface transfer doping of diamond fundamentally requires termination of the diamond surface with a species such as hydrogen to allow the interfacial charge exchange required to establish surface conductivity. Here we show the effects of varied hydrogen plasma power on the roughness and conductivity of the (100) diamond surface. Prior to hydrogen termination, substrates were etched using tailored Cl_2 + Ar and O_2 + Ar chemistries to produce a very smooth surface of ~ 0.2 nm roughness average while also removing ~ 3.4 µm from the top surface as measured by Atomic Force Microscopy (AFM). Use of etching post polishing provides an effective means of producing smoother diamond surfaces with reduced crystal damage as opposed to scaife polishing alone. By producing nominally identical etched surfaces, a relationship between surface conductivity and hydrogen termination plasma power was observed. Using MoO_3 as a surface acceptor material, Hall measurements were performed to examine sheet resistance, carrier density and mobility within the diamond. Increased surface conductivity due to enhanced hole mobility was observed at higher hydrogen plasma power conditions, despite an associated increase in roughness of the diamond surface.

For robust, high power electronics, the diamond material system shows great promise. With a wide band-gap of 5.47 eV, extremely high intrinsic breakdown field of 10 MV/cm and a high thermal conductivity of greater than 20 W/cm, diamond is potentially an excellent candidate for use in devices such as high-power and high-

frequency field effect transistors (FET) [1, 2, 3, 4, 5, 6]. Yet, the lack of a mature doping process has thus far limited exploitation of diamond's electronic potential for real world devices [7]. Surface transfer doping provides a potential solution to the doping problems in diamond, generating an abundance of research interest in recent years [8, 9, 10]. The process of transfer doping couples itself intimately with the surface of diamond. The mechanism for electron transfer relies upon a foundation of two components: hydrogen termination of the surface and contact with a suitable electron acceptor medium. Historically, this acceptor medium has been provided by spontaneous accumulation of molecular adsorbents from air *i.e.* exposing a hydrogen terminated diamond (H-diamond) substrate to ambient atmosphere would generate a dramatic increase in conductivity of the otherwise highly insulating diamond surface [11]. However, these atmospheric adsorbates are volatile, easily desorbed by elevated temperatures or exposure to chemicals and plasma during standard fabrication processes [11]. This has prompted research into alternative surface materials which act as an electron acceptor when in contact with the hydrogen terminated diamond surface. Electron withdrawing molecules such as fullerene C_{60}, its fluorinated variants ($C_{60}F_{48}$), F_4-TCNQ and several high electron affinity transition metal oxides such as Nb_2O_5, WO_3, ReO_3, V_2O_5 and MoO_3 have been shown to induce surface transfer doping in diamond [12, 13, 14, 15, 16, 17]. While these surface electron acceptors, particularly ReO_3, V_2O_5 and MoO_3, have demonstrated advanced performance, the relationship between the surface condition, topology, roughness, hydrogen coverage, defect density and the efficiency of transfer doping is still poorly understood. In this work, we present experimental results from CVD (100) diamond substrates hydrogen terminated by high-power microwave plasma using varied power density. Prior to hydrogen treatment, each substrate was etched using Inductively Coupled Plasma (ICP) and Reactive-Ion Etching (RIE) to produce nominally identical surfaces. The diamond surface was characterised by AFM measurement before and after hydrogen termination, showing surface profile and roughness, while electrical performance of each substrate was measured by way of Hall measurement using MoO_3 deposited simultaneously on each sample as a consistent surface acceptor.

Experimental

Three 'optical grade' substrates were provided by Element Six with (100) surface orientation and 3 × 3 × 0.5 mm dimensions. The samples were polished by 'Diamond Product Solutions' using a scaife wheel and for the purpose of this work are designated

A1 – A3. After polishing, each substrate was cleaned in a boiling acid solution of HNO_3:HCl followed by H_2SO_4:HNO_3 to remove any metallic and organic adsorbents. Roughness data for these samples ranged from 0.7 to 0.9 nm roughness average (Ra) and 0.9 to 1.2 nm roughness root mean squared (Rq), as measured by AFM.

The samples were then etched using a tailored Ar + Cl_2 chemistry in an Oxford Instrument PlasmaLab Inductively Coupled Plasma (ICP) etching system ICP180. The ICP etching parameters used were as follows: chamber pressure 5 mTorr, stage temperature 20°C, ICP coil power 400 W and RF platen power 10 W, Cl_2 flow rate 40 sccm and Ar flow rate 25 sccm. The etch rate for this recipe was measured as approximately 10 nm per minute using a NiCr mask, in close agreement with C. L. Lee *et al* [18]. The etching mechanism of diamond using Ar + Cl_2 plasma is reported to be: $C + Cl_2 \rightarrow CCl_x$. Ar ions sputter the diamond surface enabling the reaction of chlorine with carbon atoms to form the volatile etch product CCl_x. All three samples were etched simultaneously to a depth of approximately 3 μm. Due to the extensive etch time required as a result of the slow etch rate, the chamber was purged in cycles of 10 minutes to avoid build-up of etch product. After Ar + Cl_2 etching, surface Ra was reduced significantly to 0.4 nm for all three samples with relatively small difference between Ra and Rq, indicating a more uniform surface profile.

A further 400 nm was removed from the top surface using a Ar + O_2 etch in an Oxford Instrument PlasmaLab System-100 Reactive Ion Etcher (RIE), with the motivation of removing any possible Cl_2 contamination of the diamond surface. The RIE parameters used were as follows: chamber pressure 20 mTorr, stage temperature 22ºC, RF power 200 W, O_2 flow rate 40 sccm and Ar flow rate 10 sccm. Etch rate for this recipe was measured as approximately 25 nm per minute using a S1818 resist mask, a rate significantly faster than the Ar + Cl_2 recipe due to the highly volatile CO_x gas formation. However, this etching rate using O_2 is still significantly slower than those reported elsewhere [19], as a less aggressive process was used to avoid roughening the diamond surface. Surface Ra was reduced further to roughly 0.2 nm with small difference between Ra and Rq as a result of the very smooth profile. These samples demonstrated some of the smoothest surfaces reported for CVD single crystal diamond.

Each sample was then treated with hydrogen plasma performed in a resonant-cavity CVD diamond growth reactor (*Plassys BJS150*). The samples were placed onto a water-cooled holder and first pumped to a low base pressure below 10^{-6} mbar before purified hydrogen (9N) was

introduced at a constant flow rate of 250 sccm. The plasma power density was varied for each sample by using different microwave power and pressure. A1, A2 and A3 were treated using low, medium and high power plasma conditions corresponding to: 1.5 kW-60 mbar, 2.1 kW-110 mbar and 2.6 kW-160 mbar respectively. The temperature of the samples was maintained at 640 °C (± 30°C) for all plasma power conditions. This was achieved by adjusting the thermal contact between the Mo holder and the cooled stage through the insertion of graphite sheets. While a higher temperature for hydrogen termination is often reported in the literature, we observe good H-termination at 640ºC. This has also been reported by others [20] and is in part due to the relatively high-power densities used whereby atomic hydrogen can be produced in a large amount allowing the surface to be H-terminated at moderate temperatures. All samples were treated for the same duration of 45 minutes.

To perform electrical characterisation of the hydrogen terminated samples, van der Pauw (VDP) structures were formed by applying silver paste to the corners of each sample. Great care was taken to ensure the contacts were well formed, with good symmetry and no overflow of the sample edges. The conductivity of both sides of the samples were also measured using basic 2-probe IV measurements which only demonstrated measurable conductivity on the surface that was exposed during the H-termination process. This method of VDP formation has proven effective for Hall measurement, showing sufficiently low contact resistance with a linear IV response [21]. Use of this method also removes the risk of contaminating the diamond surface by standard fabrication techniques, such as exposure to resists and processing chemicals. After electrical contacts were formed on the sample corners, 100 nm of MoO_3 was deposited onto each sample simultaneously by thermal evaporation in a vacuum of 2×10^{-6} mbar and the oxide thickness controlled using a quartz crystal monitor during deposition. An *in-situ* annealing step of 400ºC for 1 hour immediately prior to oxide deposition was used to ensure desorption of any residual adsorbed species on the diamond surface, as reported elsewhere [14, 16]. All Hall measurements were performed by probing through the deposited oxide layer and directly onto the silver contacts using a *Nanometrics* HL5500PC Hall effect measurement system. Care was taken to ensure that proper electrical contact was made between the probes and silver contacts by monitoring the IV response between adjacent contacts.

Results and discussion

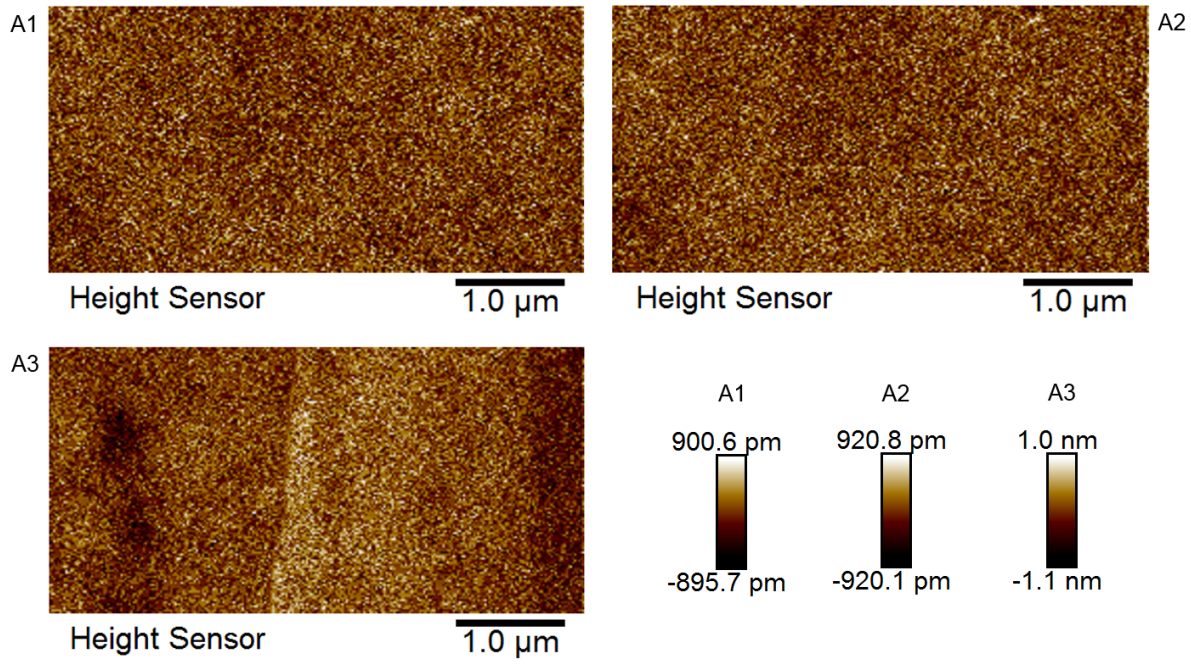

Figure 1 – 5 µm AFM surface scans of substrates A1, A2 and A3 after etching and prior to hydrogen termination.

Figure 1 shows AFM scans for samples A1 to A3 after etching and prior to hydrogen treatment. A summary of roughness values for each processing step is presented in Table 1. After each stage of etching, surface roughness is decreased and the difference in Ra and Rq reduced, achieving a smoother surface profile while also removing approximately 3.4 µm in total from the polished surface. In doing so, polishing induced crystal defects were likely removed or at least substantially reduced [22]. Figure 2 shows 3D renders of each sample after etching, accompanied by cross section plots of the surface. Figure 3 shows AFM scans for each sample after treatment in hydrogen plasma. After hydrogen termination, surface roughness was

		Polished			Ar + Cl_2 etched			Ar + O_2 etched			Hydrogen Terminated	
Sample		Ra	Rq		Ra	Rq		Ra	Rq		Ra	Rq
A1 (Low)	(nm)	0.71	0.89	↓	0.42	0.53	↓	0.21	0.26	=	0.21	0.31
A2 (Med)	(nm)	0.92	1.2	↓	0.44	0.55	↓	0.21	0.26	↑	1.2	1.6
A3 (High)	(nm)	0.85	1	↓	0.44	0.56	↓	0.24	0.3	↑	1.3	1.6

Table 1 – Summary of roughness data after each processing step for samples A1, A2 and A3.

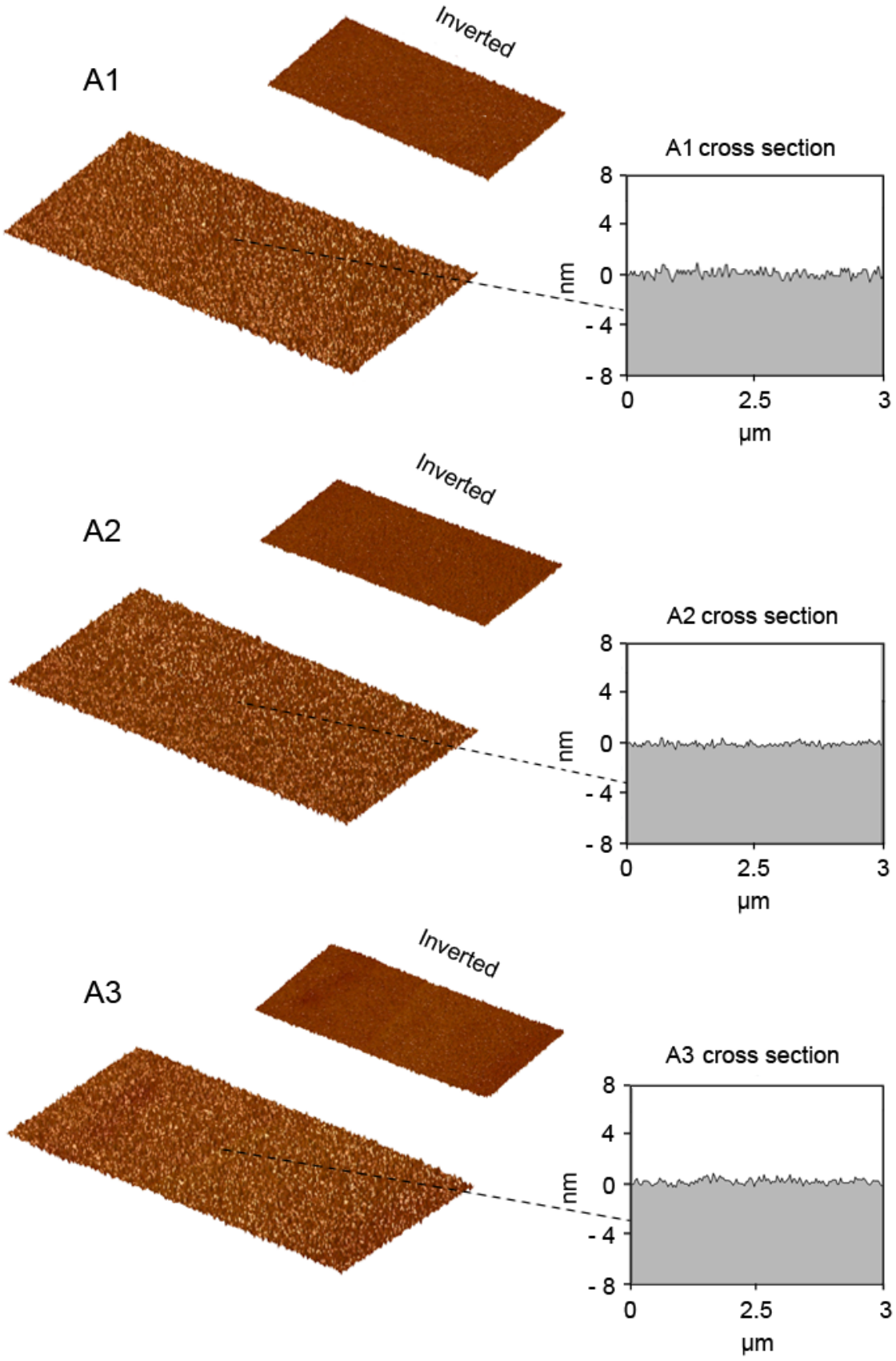

Figure 2 - 3D AFM renders of etched substrates A1, A2 and A3 prior to hydrogen termination. Cross section plots of the surface are shown, taken parallel to the scan direction (x-axis).

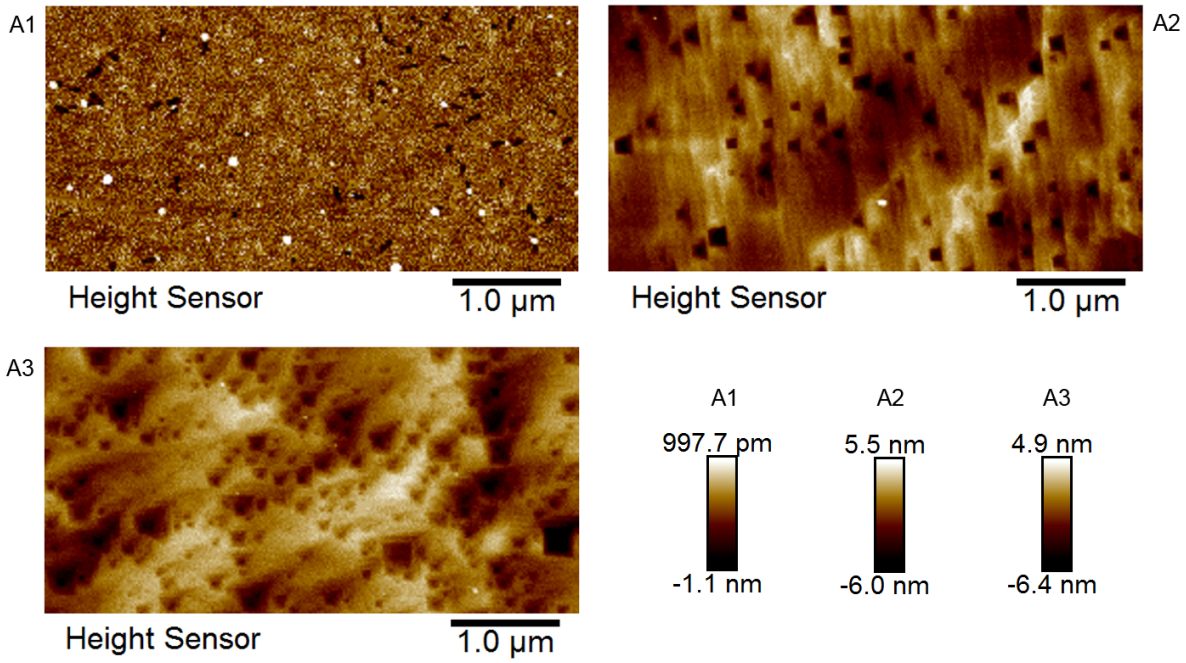

Figure 3 – 5 µm AFM surface scans of substrates A1, A2 and A3 after treatment in hydrogen plasma.

significantly increased for samples A2 and A3. However, the lower plasma-power sample A1 remained mostly unchanged with only slight roughening. Figure 4 shows 3D renders of AFM scans for samples A1-A3 after hydrogen treatment, accompanied by inverted images and cross section profiles of select pit sites induced by the hydrogen termination process on each surface. A clear progression in pit width and depth can be seen between samples, as increased hydrogen plasma power most likely resulted in greater etching of defect sites despite the absence of oxygen [23]. The formation of etch pits in samples A2 and A3 appear to be from bulk defects incurred during CVD growth, as polishing induced defects were likely removed during etching [19]. Polishing defects have also been previously observed to follow the direction of the polishing wheel, which is not seen here [24]. The formation of such pits on the surface of diamond after hydrogen plasma treatment is a known phenomenon; work by Naamoun *et al* showed defects at the diamond surface can be revealed by H_2/O_2 etching with relatively low amounts of oxygen [25]. They also found these defects present as pits in the form of hollow inverted pyramids. Their work concluded two main sources of these pits; firstly, crystal dislocations at the surface introduced by polishing and secondly, dislocations that originate from defects in the bulk of the material. These

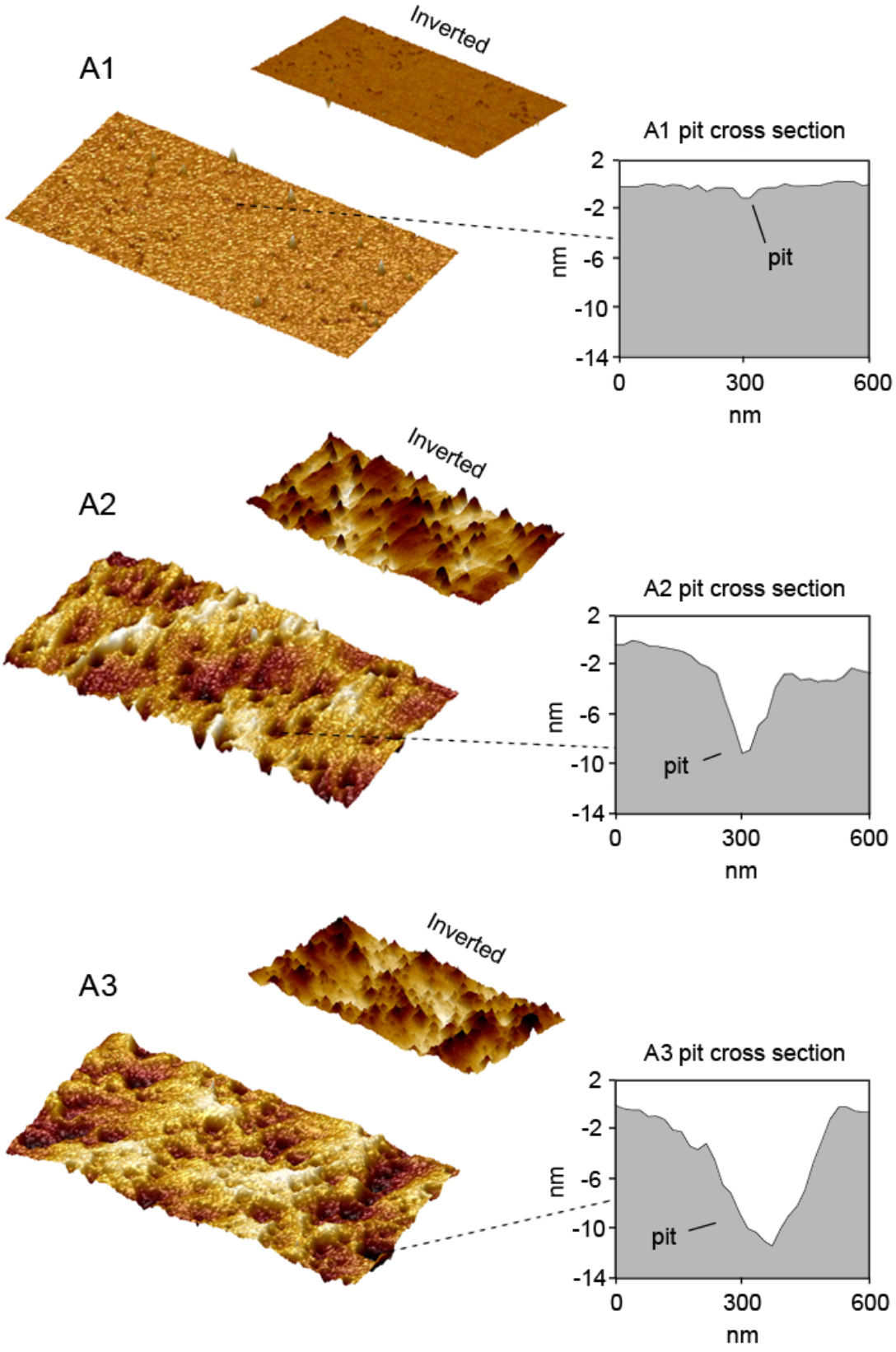

Figure 4 - 3D AFM renders of etched substrates A1, A2 and A3 after hydrogen termination. Progression of pit formation is shown to increase with plasma power density. Cross sections are taken parallel to the scan direction (x-axis).

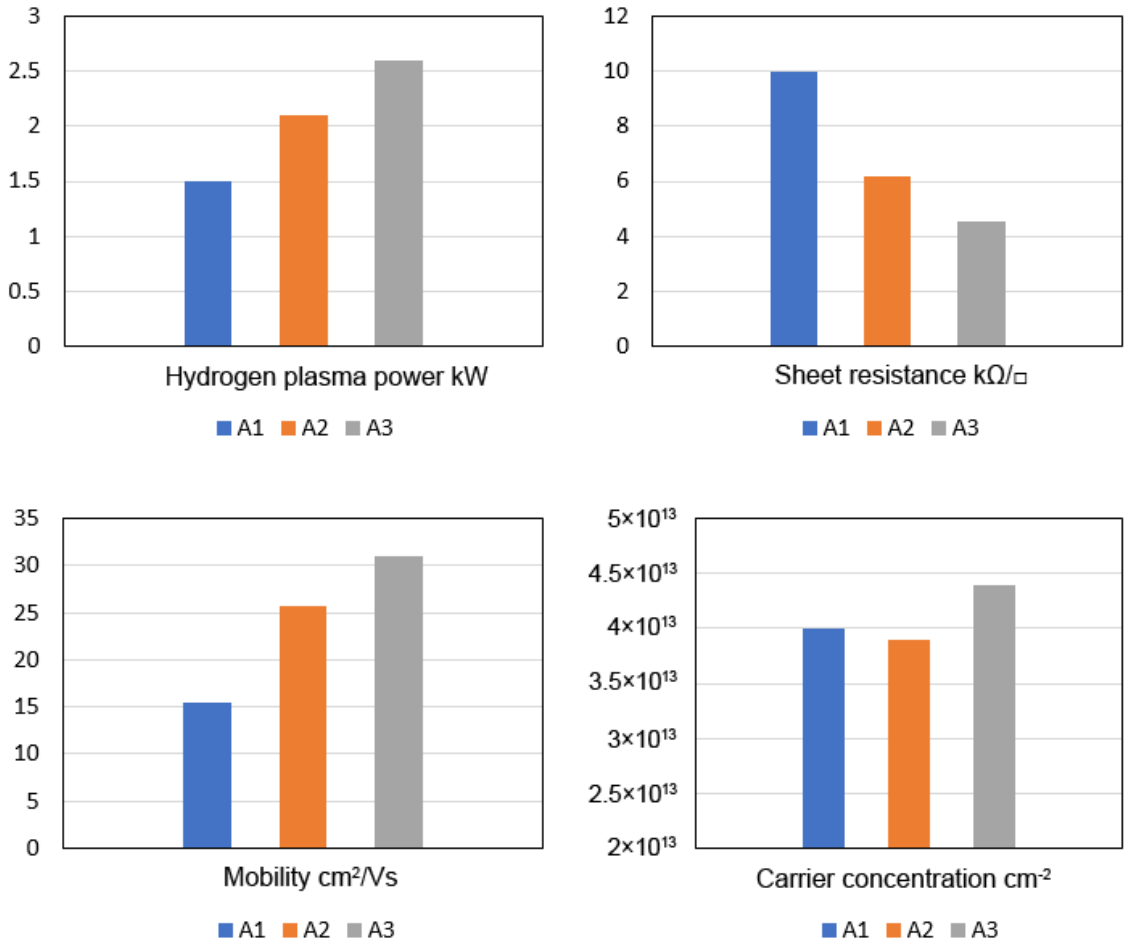

Figure 5 – Graphical presentation of Hall measurement results with termination power for samples A1, A2 and A3.

non-sp^3 bonded defects at the surface are susceptible to etching by atomic hydrogen produced in the plasma, especially when relatively high-power densities are used. Defects such as dislocations and stacking faults are common in both synthetic and natural diamond [26] and have previously been observed in Element six CVD material [27]. Tallaire *et al* also showed aggressive H_2/O_2 plasma exposure could reveal defects at the surface and presented cross sections of different pit geometries. They concluded a range of defect types once etched would present differently and that polishing induced defects could be removed by ICP etching such that only bulk dislocations are left [19].

VDP Hall measurements after hydrogen termination and deposition of 100 nm MoO_3 on substrates A1-A3 are shown in Figure 5. All three samples showed similar carrier density at around 4×10^{13} cm^{-2}. However, sheet resistance varied significantly from 10 kΩ/□ for the lower

plasma power sample A1 to 4.6 kΩ/□ for the higher plasma power sample A3. This difference is attributed to the much-improved mobility of sample A3 (31.1 cm^2/Vs), roughly double that of sample A1 (15.4 cm^2/Vs), while sample A2 lies roughly in- between. These results suggest a higher termination power when applied to three nominally identical samples produces improved carrier mobility, while carrier density remains largely similar for all three. The mechanism for improved mobility here is unclear, however the higher power termination used on sample A3 produced a notably higher surface roughness with ~ 6 times the surface Ra of sample A1. Samples A2 and A3 exhibited similar average roughness, yet a distinctly different presentation of surface topology with sample A3 presenting larger, more numerous and varied etch pit locations as can be seen in Figures 3 & 4. In this instance, increased surface roughness (at least for the scales investigated here) would appear to enhance the hole mobility in the sub-surface 2-dimensional hole gas (2DHG) within the diamond. This result is rather counter intuitive, as surface/interface roughness scattering is well known to negatively impact carrier mobility in other material systems [28, 29, 30]. Part of the explanation for our observations may be linked to the removal of surface defect sites by the more aggressive hydrogen plasma conditions, as the impact of such defects on carrier transport in surface transfer doped hydrogen terminated diamond is not yet well understood. T. Wade *et al* also observed increased surface conductivity with increased surface roughness in single crystal hydrogen terminated diamond with (100) orientation [31]. However, they attributed this increase in conductivity to an increase in 'activation sites' which in turn led to an increase in carrier density rather than mobility. This group utilised a different surface acceptor in their work in the form of NO_2 atmosphere rather than MoO_3 as we report here. The range of surface roughness investigated is also substantially higher than we report here (Rq from ~ 5 nm to 450 nm). Although we also observe a similar increase in conductivity with increased surface roughness, the variation in substrate preparation, surface acceptor material, surface roughness range and carrier density between these works therefore makes direct comparison of the results difficult. However, both indicate that carrier density and transport in transfer doped H-diamond seem to be closely linked to the surface morphology. Some etch pits on the CVD diamond surface have been reported to exhibit side walls with (111) orientation [32]. Work by K. Hirama *et al* observed reduced sheet resistance for CVD diamond with (111) surface orientation, attributed to a higher dipole density compared to that of the (100)

surface [33]. However, this effect of reduced sheet resistance is due to increased carrier density as opposed to improved mobility as observed in this work.

Regardless of the variation in the surface conditions, a direct relationship between increased hole density and reduced carrier mobility has been consistently reported for surface transfer doped hydrogen terminated diamond [12, 14, 15, 34]. This suggests that carrier mobility in H-diamond may be limited by proximity to the surface in the form of surface roughness or Coulomb scattering from electrons within the surface acceptor layer i.e. the average separation between the charge in the 2DHG and the diamond surface will be reduced at higher carrier densities due to deepening and narrowing of the surface triangular-like potential well. This model assumes that electrons transferred to the MoO_3 layer remain localised at the diamond/oxide interface and do not significantly contribute to the observed current flow – an assumption supported by the consistent Hall measurement of p-type conductivity in these systems [15]. Beyond the potential removal of mobility-degrading defect sites, the enhanced carrier mobility observed in the roughest sample, A3, may therefore also be linked to a reduction in Coulomb scattering associated with increased average separation between the fixed charge in the surface acceptor and mobile charge in the diamond due to increased surface roughness. This hypothesis suggests there exists a potentially complex relationship between carrier mobility and surface morphology in H-diamond whereby mobility enhancement may be achievable through engineering of the surface topography. However, collection of a more expanded dataset beyond the preliminary results presented is required to better understand and exploit this potential phenomenon. Nevertheless, these initial findings introduce some exciting prospects for the production of enhanced mobility electronic devices in H-diamond.

Conclusions

A process for the production of smooth diamond surfaces after scaife polishing by way of ICP and RIE etching has been detailed, achieving surface roughness of ~ 0.2 nm and reducing the impact of polishing-induced crystal damage. Using this process to prepare three nominally identical sample surfaces, the effects of varied plasma power density during hydrogen termination on sample roughness and conductivity has been shown. After removing ~3.4 μm for the top diamond surface by etching, increasing plasma power density was found to produce a significantly rougher surface. The mechanism for this increased roughness most likely comes from the selective etching of surface defects by

atomic hydrogen during a more aggressive hydrogen termination process. However, the rougher surfaces produced by harsher hydrogen termination also exhibited reduced sheet resistance due to higher carrier mobility while also producing similar levels of carrier density between samples. The mechanism by which carrier mobility is increased with increased surface roughness is not yet understood, but may be linked to removal of surface defects as part of a more aggressive hydrogen-termination process. The relationship between surface roughness and charge mobility in H-diamond is also presently little understood, and may play an additional and more complex role in these results. Further investigation into these processes is required to better understand the intimate and potentially complex relationship between the surface and charge carrier properties in transfer-doped hydrogen-terminated diamond.

The authors wish to acknowledge the James Watt Nanofabrication Centre for making this work possible. DQ acknowledges the support of the Australian Research Council (Grant No. DP150101673 and FT160100207). DM wishes to thank the EPSRC (EP/E054668/1) for funding.

[1] C. J. H. Wort and R. S. Balmer, Diamond as an electronic material, Mater. Today 11, 22 (2008)

[2] K. Hirama, H. Takayanagi, S. Yamauchi, Y. Jingu, H. Umezawa, and H. Kawarada, High-performance p-channel diamond MOSFETs with alumina gate insulator IEDM Technical Digest (2007)

[3] Stephen Russell, Salah Sharabi, Alexandre Tallaire, David A. J. Moran, RF Operation of Hydrogen-Terminated Diamond Field Effect Transistors: A Comparative Study, IEEE Transactions on Electron Devices, 62, 751 – 756, 2015

[4] M. Kasu and T. Oishi, Recent Progress of Diamond Devices for RF Applications IEEE Compound Semiconductor Integrated Circuit Symposium (CSICS), Austin, TX, (2016)

[5] Kawarada, Hiroshi, Yamada, Tetsuya, Xu, Dechen, Tsuboi, Hidetoshi, Kitabayashi, Yuya, Matsumura, Daisuke, Shibata, Masanobu, Kudo, Takuya, Inaba, Masafumi, Hiraiwa, Atsushi, Durability-enhanced two-dimensional hole gas of C-H diamond surface for complementary power inverter applications, Scientific Reports, 7, 42368, (2017).

[6] Yuya Kitabayashi, Takuya Kudo, Hidetoshi Tsuboi, Tetsuya Yamada, Dechen Xu, Masanobu Shibata, Daisuke Matsumura, Yuya Hayashi, Mohd Syamsul, Masafumi Inaba, Atsushi Hiraiwa, Hiroshi Kawarada, Normally-Off C-H Diamond MOSFETs with Partial C-O Channel Achieving 2-kV Breakdown Voltage, IEEE Electron Device Lett. 38, 363-366 (2017).

[7] M. E. Zvanut, Shigang Zhang and W. E. Carlos, A Study of Dopants in Diamond Using Electron Paramagnetic Resonance Spectroscopy, MRS Proceedings, 416, (1995)

[8] Wei Chen, Dongchen Qi, Xingyu Gao, Andrew T. S. Wee, Surface transfer doping of semiconductors, Progress in Surface Science 84, 279–321, (2009)

[9] Christopher I. Pakes, Jose A. Garrido, Hiroshi Kawarada, Diamond surface conductivity: Properties, devices, and sensors, MRS Bulletin, 39, 6, 542-548 (2014)

[10] J. Ristein, Diamond surfaces: familiar and amazing, Appl. Phys. A 82, 377–384 (2006)

[11] F. Maier, M. Riedel, B. Mantel, J. Ristein and L. Ley, Origin of Surface Conductivity in Diamond, Physics Review Letters, 85, (2000)

[12] Qi, D., Chen, W., Gao, X., Wang, L., Chen, S., Loh, K. P., Wee, A. T. S. Surface Transfer Doping of Diamond (100) by Tetrafluoro-tetracyanoquinodimethane, JACS, 129, 8084-8085 (2007).

[13] Tordjman, M., Saguy, C., Bolker, A., Kalish, R. Superior Surface Transfer Doping of Diamond with MoO3, Adv. Mater. Interfaces, 1, 1300155 (2014).

[14] Crawford, K. G., Cao, L., Qi, D., Tallaire, A., Limiti, E., Verona, C., Wee A. T. S., Moran, D. A. J. Enhanced surface Transfer Doping of Diamond by V2O5 with Improved Thermal Stability, Appl. Phys. Lett., 108, 042103 (2016).

[15] Russell, S. A. O., Cao, L., Qi, D., Tallaire, A., Crawford, K. G., Wee, A. T. S., Moran, D. A. J. Surface Transfer Doping of Diamond by MoO3: A Combined Spectroscopic and Hall Measurement Study, Appl. Phys. Lett., 103, 202112 (2013).

[16] Verona, C., Ciccognani, W., Colangeli, S., Limiti, E., Marinelli, M., Verona-Rinati G., Cannatà, D., Benetti, M., Pietrantonio, F. D. V2O5 MISFETs on H-Terminated Diamond, IEEE Trans. on Elec. Devi., 63, 4647-4653 (2016).

[17] Moshe Tordjman, Kamira Weinfeld, Rafi Kalish, Boosting surface charge-transfer doping efficiency and robustness of diamond with WO3 and ReO3, Appl. Phys. Lett. 111, 111601 (2017)

[18] C. L. Lee, E. Gu, M. D. Dawson, I. Friel, G. A. Scarsbrook, “Etching and micro-optics fabrication in diamond using chlorine-based inductively-coupled plasma” Diamond and Related Materials, 17, (2008)

[19] Alexandre Tallaire, Thierry Ouisse, Arthur Lantreibecq, Robin Cours, Marc Legros, Hakima Bensalah, Julien Barjon, Vianney Mille, Ovidiu Brinza, and Jocelyn Achard, Identification of Dislocations in Synthetic Chemically Vapor Deposited Diamond Single Crystals, Cryst. Growth Des., 16, 2741−2746 (2016)

[20] M. Kubovic, M. Kasu, Enhancement and Stabilization of Hole Concentration of Hydrogen-Terminated Diamond Surface

Using Ozone Adsorbates, Japanese Journal of Applied Physics, 49 (2010) 110208

[21] Rossi, M. C., Spaziani, F., Salvatori, S., Conte, G. Electronic Properties of Hydrogen and Oxygen Terminated Surfaces of Polycrystalline Diamond Films, Phys. Status Solidi, 199, 71-76 (2003).

[22] J. Achard, A. Tallaire, V. Mille, M. Naamoun, O. Brinza, A. Boussadi, L. William, A. Gicquel, Improvement of dislocation density in thick CVD single crystal diamond films by coupling H2/O2 plasma etching and chemo-mechanical or ICP treatment of HPHT substrates, physica status solidi (a), 211, 2264-2267, (2014)

[23] K. Ichikawa, H. Kodama, K. Suzuki, A. Sawabe, Dislocation in heteroepitaxial diamond visualized by hydrogen plasma etching, Thin Solid Films, 600 (2016) 142-145.

[24] M.P. Gaukroger, P.M. Martineau, M.J. Crowder, I. Friel, S.D. Williams, D.J. Twitchen, X-ray topography studies of dislocations in single crystal CVD diamond, Diamond & Related Materials 17, 262–269, (2008)

[25] M. Naamoun, A. Tallaire, F. Silva, J. Achard, P. Doppelt, A. Gicquel, Etch-pit formation mechanism induced on HPHT and CVD diamond single crystals by H_2/O_2 plasma etching treatment, Phys. Sta. Soli, 209, (2012)

[26] N. Tsubouchi, Y. Mokuno, S. Shikata, Characterizations of etch pits formed on single crystal diamond surface using oxygen/hydrogen plasma surface treatment, Diamond and Related Materials, 63, (2016)

[27] I. Friel, S.L. Clewes, H.K. Dhillon, N. Perkins, D.J. Twitchen, G.A. Scarsbrook, Control of surface and bulk crystalline quality in single crystal diamond grown by chemical vapour deposition, Diam. & Relat. Mat., 18 (2009) 808-815

[28] S. Gökden, R. Barana, N. Balkan, S. Mazzucato, The effect of interface roughness scattering on low field mobility of 2D electron gas in GaN/AlGaN heterostructure, 24, 4, 249-256, (2004)

[29] M. N. Gurusinghe, S. K. Davidsson, and T. G. Andersson, Two-dimensional electron mobility limitation mechanisms in AlxGa1−xN/GaN heterostructures, PHYSICAL REVIEW B 72, 045316 (2005)

[30] V K Karavolas, M J Smith, T M Fromhold, P N Butcher, B G Mulimani, B L Gallagher and J P Oxley, The effect of interface roughness scattering and background impurity scattering on the thermopower of a 2DEG in a Si MOSFET, J. Phys.: Condens. Matter 2, 10401, (1990)

[31] T.Wade, M.W.Geis, T.H.Fedynyshyn, S.A.Vitale, J.O.Varghese, D.M.Lennon, T.A.Grotjohn, R.J.Nemanich, M.A.Hollis, Effect of surface roughness and H–termination chemistry on diamond's semiconducting surface conductance, Diam. Relat. Mater. 76, 79-85, (2017)

[32] A. Tallaire, M. Kasu, K. Ueda, T. Makimoto, Origin of growth defects in CVD diamond epitaxial films, Diamond & Related Materials 17 60–65 (2008)

[33] K. Hirama, K. Tsuge, S. Sato, T. Tsuno, Y. Jingu, S. Yamauchi, and H. Kawarada, High-Performance P-Channel Diamond Metal–Oxide–Semiconductor Field-Effect Transistors on H-Terminated (111) Surface. Appl. Phys. Express, 3, 044001 (2010).

[34] H. J. Looi, R. B. Jackman, and J. S. Foord, High carrier mobility in polycrystalline thin film diamond, Appl. Phys. Lett. 72, 353 (1998)